

This is a repository copy of *The impact of gape on the performance of the skull in chisel-tooth digging and scratch digging mole-rats (Rodentia: Bathyergidae)*.

White Rose Research Online URL for this paper:

<https://eprints.whiterose.ac.uk/id/eprint/104173/>

Article:

McIntosh, Andrew and Cox, Philip Graham orcid.org/0000-0001-9782-2358 (2016) The impact of gape on the performance of the skull in chisel-tooth digging and scratch digging mole-rats (Rodentia: Bathyergidae). Royal Society Open Science. 160568. ISSN: 2054-5703

<https://doi.org/10.1098/rsos.160568>

Reuse

Items deposited in White Rose Research Online are protected by copyright, with all rights reserved unless indicated otherwise. They may be downloaded and/or printed for private study, or other acts as permitted by national copyright laws. The publisher or other rights holders may allow further reproduction and re-use of the full text version. This is indicated by the licence information on the White Rose Research Online record for the item.

Takedown

If you consider content in White Rose Research Online to be in breach of UK law, please notify us by emailing eprints@whiterose.ac.uk including the URL of the record and the reason for the withdrawal request.

ROYAL SOCIETY
OPEN SCIENCE

**The impact of gape on the performance of the skull in
chisel-tooth digging and scratch digging mole-rats
(Rodentia: Bathyergidae)**

Journal:	<i>Royal Society Open Science</i>
Manuscript ID	RSOS-160568.R1
Article Type:	Research
Date Submitted by the Author:	28-Aug-2016
Complete List of Authors:	McIntosh, Andrew; University of Hull, Hull York Medical School Cox, Philip Graham; University of York, Department of Archaeology; University of York, Hull York Medical School
Subject:	biomechanics < PHYSICS, evolution < BIOLOGY
Keywords:	Cranial biomechanics, Finite element analysis, Chisel-tooth digging, Scratch digging, Bathyergidae
Subject Category:	Biology (whole organism)

SCHOLARONE™
Manuscripts

Responses to reviewers

We thank the reviewers for their positive comments on the manuscript. We have addressed the outstanding issues as follows:

1. The spelling of the species name of *Fukomys mechowii* has now been corrected throughout the manuscript.
2. The Barciova et al paper on the relationship between soil type and cranial morphology has now been discussed and cited in both the introduction (line 70) and conclusions (line 335).
3. Apologies for giving the wrong Figshare link – I’m still getting to grips with the site. The correct link has been added to the manuscript and is https://figshare.com/articles/Mole_rat_FEA/3188830

Regards,

Andrew McIntosh & Phil Cox

Title: The impact of gape on the performance of the skull in chisel-tooth digging and scratch digging mole-rats (Rodentia: Bathyergidae)

Running head: Bathyergid cranial performance

Authors:

Andrew F. McIntosh¹

Philip G. Cox^{2,3}

Institutional addresses:

¹Centre for Anatomical and Human Sciences, Hull York Medical School, University of Hull, Hull, UK

²Centre for Anatomical and Human Sciences, Hull York Medical School, University of York, York, UK

³Department of Archaeology, University of York, York, UK

Corresponding author:

Philip G. Cox

Email address: philip.cox@hyms.ac.uk

Telephone: +44 1904 321744

1
2
3
4
5
6
7
8
9
10
11
12
13
14
15
16
17
18
19
20
21
22
23
24
25
26
27
28
29
30
31
32
33
34
35
36
37
38
39
40
41
42
43
44
45
46
47
48
49
50
51
52
53
54
55
56
57
58
59
60

26 **ABSTRACT**

27 The African mole-rats (Bathyergidae) are a family of rodents highly adapted for life
28 underground. Previous research has shown that chisel-tooth digging mole-rats (which use
29 their incisors to dig burrows) are clearly distinguishable from scratch diggers (which only use
30 the forelimbs to tunnel) on the basis of morphology of the skull, and that the differences are
31 linked to the production of high bite forces and wide gapes. We hypothesised that the skull of
32 a chisel-tooth digging mole-rat would perform better at wider gapes than that of a scratch
33 digging mole-rat during incisor biting. To test this hypothesis, we created finite element
34 models of the cranium of the scratch digging *Bathyergus suillus* and the chisel-tooth digging
35 *Fukomys mechowii*, and loaded them to simulate incisor bites at different gapes. Muscle loads
36 were scaled such that the ratio of force to surface area was the same in both models. We
37 measured three performance variables: overall stress across the cranium; mechanical
38 efficiency of biting; and degree of deformation across the skull. The *Fukomys* model had a
39 more efficient incisor bite at all gapes, despite having greater average stress across the skull.
40 In addition, the *Fukomys* model deformed less at wider gapes, whereas the *Bathyergus* model
41 deformed less at narrower gapes. These properties of the cranial morphology of *Fukomys*
42 and *Bathyergus* are congruent with their respective chisel-tooth and scratch digging
43 behaviours and, all other factors being equal, would enable the more efficient production of
44 bite force at wider gapes in *Fukomys*. However, *in vivo* measurements of muscle forces and
45 activation patterns are needed to fully understand the complex biomechanics of tooth digging.

47 **Keywords: Cranial biomechanics; finite element analysis; chisel-tooth digging; scratch**
48 **digging; Bathyergidae**

51 INTRODUCTION

52 The African mole-rats, or blesmols, are a family of rodents (Bathyergidae) comprising 25-30
53 species, all of which spend a large proportion of their life underground [1]. Of the six extant
54 genera, five are chisel-tooth diggers, that is, they dig tunnels with their enlarged rodent
55 incisors. Just one genus (*Bathyergus*) is a scratch digger, tunnelling with only its forelimbs
56 and claws [2]. Chisel-tooth digging is a specialised form of tunnel construction that has also
57 evolved independently in several other families of subterranean and fossorial rodents [3]. It is
58 thought to have evolved in order to exploit harder soils as incisors are covered in hard enamel
59 and fixed within the cranium and mandible. This is in contrast to the claws, which are made
60 up of softer keratin and have more flexibility [4].

62 A number of morphological characteristics in the cranium have been associated with chisel-
63 tooth digging. These include: more procumbent incisors, wider crania, enlarged zygomatic
64 arches and larger temporal fossae [5-9]. Chisel-tooth digging mandibles are also convergent
65 across rodents and show higher coronoid processes, reduced condyle heights and deep incisor
66 roots [6,10,11]. Such traits have been linked to the requirement for chisel-tooth diggers to
67 produce high bite force at the incisors at wide gape [5,6,10], and have also been found in
68 carnivorans with similar functional requirements [12-14]. Within chisel-tooth digging
69 species, variation in cranial morphology has been suggested to correlate with soil type,
70 indicating that digging has a major influence on skull shape [15,16].

72 To understand how morphological traits can impact biomechanical function in extant and
73 extinct vertebrates, many researchers have turned to the engineering technique finite element
74 analysis (FEA) over the decade or so [17-26]. FEA allows stress, strain and deformation to be
75 predicted in a complex 3D object subjected to a load, by dividing that object into a large

1
2
3
4
5
6
7
8
9
10
11
12
13
14
15
16
17
18
19
20
21
22
23
24
25
26
27
28
29
30
31
32
33
34
35
36
37
38
39
40
41
42
43
44
45
46
47
48
49
50
51
52
53
54
55
56
57
58
59
60

76 number of smaller, simpler elements (usually cubes or tetrahedra) connected at nodes [27].
77 As a modelling technique, the results of FEA, and the conclusions that can be drawn from
78 them, are necessarily limited by the accuracy of the model inputs. In particular, parameters
79 such as material properties, constraints and loads are often unknown or can only be roughly
80 estimated in biological models. Indeed, some validation studies have indicated that outputs
81 from FEA (e.g. strain values) do not always match *ex vivo* or *in vivo* measurements in
82 absolute terms [18,28,29]. However, these studies also indicate that the relative values are
83 generally correct (e.g. areas of high strain and low strain predicted by FEA match those
84 measured *in vivo*). Thus, whilst comparisons of absolute values between different unvalidated
85 FE models can be difficult to interpret, comparisons between different loading scenarios in
86 the same model (i.e. where one parameter is varied but all others are held constant) are
87 justified.

88

89 The aim of this study is to predict the performance of the skull of two bathyergid mole-rats,
90 one chisel-tooth digger and one scratch digger, when loaded at the incisors over a number of
91 different gapes. It is hypothesised that the shape of the cranium of the chisel-tooth digging
92 species will lead to improved performance at the incisors compared to the scratch digging
93 species, particularly at wide gapes. FEA will be used to simulate masticatory muscle loading
94 at different gape angles, and the patterns of stress distribution across the cranium will be
95 predicted, as well as bite force at the incisors. By integrating geometric morphometrics
96 (GMM) with FEA [22,30], it will also be possible to quantify and visualise the differences in
97 overall deformations of the cranium between the two species. Following Dumont *et al.* [20],
98 biomechanical performance will be measured in three ways. We predict that, compared to the
99 scratch digging species, the chisel-tooth digging cranial model at wide gapes will: (1) exhibit
100 lower stress (and thus be more resistant to structural failure); (2) be more efficient at

101 converting muscle forces to bite forces; and (3) experience less deformation. These
102 predictions are based on the hypothesis that the cranial morphology of the chisel-tooth
103 digging mole-rat will be adapted to both generate high forces at the incisors and withstand the
104 reaction forces. It should be noted that this analysis seeks only to understand the impact of
105 the difference in cranial morphology between *Fukomys* and *Bathyergus*. Many other factors
106 can influence digging biomechanics, such as muscle physiology, muscle activation patterns
107 and bone material properties, but data on these is scant in mole-rats and they are beyond the
108 focus of this study.

109

110 MATERIALS AND METHODS

111 *Model construction*

112 Finite element (FE) models were created from microCT scans of two adult African mole-rat
113 skulls: the chisel-tooth digging *Fukomys mechowii* (Muséum National d'Histoire Naturelle,
114 Paris, ZM-MO-1911-664) and the scratch digging *Batherygus suillus* (Specimen 631,
115 Professor Nigel Bennett, University of Pretoria). The specimens were scanned in an X-Tek
116 Metris microCT scanner at the University of Hull (Medical and Biological Engineering
117 Research Group). The scans had isometric voxels of 0.0417 mm (*Fukomys*) and 0.0532 mm
118 (*Bathyergus*). Using Avizo 8.0 (FEI, Hillsboro, OR) the scans were resampled to double their
119 original voxel sizes to ensure a reasonable processing time during FE model creation and
120 solving stages. 3D volume reconstructions of the skulls were created by a combination of
121 automated and manual thresholding of materials. Bone, teeth, and incisor pulp cavity were
122 segmented as separate volumes, with all bone was modelled as cortical bone. The
123 reconstructions were then converted to an 8-noded cubic mesh directly from voxels using
124 VOX-FE, in-house custom-built FEA software [31]. The *Fukomys* and *Bathyergus* models
125 comprised 9481075 and 6796670 elements, respectively.

1
2
3 126
4
5 127 Based on previous nano-indentation work on rodents [21,32] and other mammals [19], bone
6
7 128 and teeth were assigned Young's moduli of 17 and 30 GPa, respectively. Pulp was assigned a
8
9 129 Young's modulus of 2 MPa [33]. All materials were modelled as homogeneous and isotropic
10
11 130 with a Poisson's ratio of 0.3 being assigned to bone and teeth and a ratio of 0.45 to pulp [33].
12
13 131 No data is available for material properties of bathyergids. However, it was considered
14
15 132 appropriate to use these properties as this study is primarily concerned with the relative
16
17 133 digging performance between two species, and therefore is less concerned with absolute
18
19 134 output values.
20
21
22 135
23
24 136 In order to model chisel-tooth digging, the models were constrained at the point of contact of
25
26 137 the incisor tip with the substrate in the direction of the bite (i.e. orthogonal to the occlusal
27
28 138 plane). Forty nodes were constrained at each temporo-mandibular joint (TMJ) in all three
29
30 139 axis. Loads were added to the model representing the following muscles: temporalis;
31
32 140 superficial masseter; deep masseter; zygomaticomandibularis (ZM: infraorbital, anterior and
33
34 141 posterior parts); lateral pterygoid; and medial pterygoid (Figure 1). The masseter muscle was
35
36 142 divided into 3 parts (superficial; deep and ZM) following [34,35]. Muscle attachment sites
37
38 143 were assigned based on previously published dissections [36-38] and virtual muscle
39
40 144 reconstructions [39] of bathyergids. Equal loads were applied to each side of the model as
41
42 145 many rodents have demonstrated a bilateral muscle activation pattern when biting at the
43
44 146 incisors [40,41].
45
46 147
47
48
49
50
51 148 The direction of pull of each muscle (i.e. muscle directional vector) was determined by
52
53 149 placing a reconstruction of the specimen's mandible in a position of incisor occlusion (0°)
54
55 150 with the cranial reconstruction using Avizo. Landmarks were placed at the centroid of each
56
57
58
59
60

muscle attachment site on the mandible. These landmarks were then uploaded into VOX-FE to provide end points for the muscle direction vectors. The *Bathyergus* and *Fukomys* mandibles were automatically segmented in Avizo from microCT scans (0.0481 and 0.0350 mm isometric voxel sizes, respectively). To calculate muscle magnitudes, PCSA values for *Fukomys mechowii* were taken from Van Daele *et al.* [38] and then multiplied by an intrinsic muscle stress value of 0.3 Nmm^{-2} [42]. No PCSA data was available for *Bathyergus*, so the *Fukomys* muscle forces, scaled to model size, were used instead (the details and limitations of this are discussed below). Muscle loads for each model are given in Table 1. To replicate different angles of gape, muscle directional vectors were rotated about an axis running between the left and right TMJ (see [6] for further details of method). Condyle translation has been shown to occur in the terrestrial rodent, *Pedetes capensis* during different stages of mastication [40]. However, condyle movement during digging at the incisors has been shown to be stable in *Ctenomys*, a South American subterranean rodent [11]. For this reason, condyle translation has not been included in the model, and the mandible has been simply rotated around an axis (TMJ).

Analysis

In this study, von Mises (VM) stress was used as a key indicator of performance. Structures which exhibit overall lower VM stresses in a comparative context are less likely to fail under a given loading. If two models of the same shape but of different sizes have equal loads, the larger model will exhibit less stress (as stress equals force applied over the area of the model). To consider the effect of difference in shape on stress between two models, the effect of size must be controlled for, which can be achieved by keeping the ratio of force to surface area constant between the two models [43]. As PCSA values were not available for *Bathyergus*, surface areas for both models were calculated in Avizo, and the ratio of the two

1
2
3
4
5
6
7
8
9
10
11
12
13
14
15
16
17
18
19
20
21
22
23
24
25
26
27
28
29
30
31
32
33
34
35
36
37
38
39
40
41
42
43
44
45
46
47
48
49
50
51
52
53
54
55
56
57
58
59
60

176 surface areas was used to scale forces applied to the *Bathyergus* model. Thus the impact of
177 cranial morphology on VM stress values for each model could be directly compared without
178 the confounding influence of size. In order to quantify VM stress across the skull, the VM
179 stress of each element from each model was extracted and the median VM stress for both
180 models was calculated. Using the median, rather than the mean, to compare VM stress
181 prevents outlying values that can arise from modelling artifacts from exaggerating the
182 average stress value.

183

184 The mechanical efficiency of incisor biting in each model was also calculated to assess the
185 performance of both models. Mechanical efficiency is the ratio of predicted bite force to total
186 muscle input force and provides a single value, independent of size, to assess the efficiency
187 of the masticatory system in transforming muscle to bite force [20,21]. Absolute bite force
188 was not reported in this study as the muscle forces and geometry of the *Fukomys* model were
189 gleaned from separate specimens. Therefore, there is no expectation that the bite force will be
190 biologically accurate. However, dividing bite force by input muscle force to produce
191 mechanical efficiency produces a meaningful performance parameter for comparison
192 between FE models.

193

194 Geometric morphometrics (GMM) was used to analyse variation in deformations between the
195 FE models, following [22,23,26,30,31,44]. A set of 3D landmarks (Figure 2 and Table S1)
196 were recorded from the unloaded and loaded models. The landmarks were then subjected to a
197 generalised Procrustes analysis and scaled to centroid size. The residual differences between
198 the loaded and unloaded models were then added to the mean landmark configuration of the
199 unloaded *Fukomys* and *Bathyergus* models. The mean and loaded configurations were
200 subjected to a second Procrustes analysis without scaling or tangent projection [44], to

represent the multivariate data on a graph. Cranial deformations were visualised via surface rendering of a hybrid of the two unloaded models warped along the vectors of deformation. Deformations were magnified 500 times to aid visual interpretation of transformation grids. All GMM analyses were carried out using the EVAN toolbox (www.evan-society.org). Further details of the GMM methods and the theory underlying them are given in electronic supplementary material, text S1.

It should be noted that because no muscle PCSA data was available for the individuals from which the model geometries were constructed, the resulting data should not be treated as reflecting biological reality. The scaling of the muscle forces instead allows us to draw conclusions on the relative impact of changing muscle orientations in species with different cranial morphologies.

RESULTS

Figure 3 shows the distribution of VM stress across the crania of the two models. As might be expected, at occlusion both models show areas of high stress around the constraints (glenoid fossae and incisor tips), and some of the muscle attachment sites (zygomatic arch and pterygoid fossa). Beyond these areas, both models also show high stresses in the postero-ventral part of the rostrum. In addition, the *Fukomys* cranium has high stresses in the dorsal rostrum and in the incisor itself. As gape increases, stress tends to decrease in the rostrum and anterior zygomatic arch, and increase in the temporal region and posterior orbital region. Studying median VM stresses (Table 2) shows that increasing gape reduces the overall stress in the cranium, and that *Fukomys* experiences higher VM stress in the cranium at each pairwise gape compared to *Bathyergus*.

1
2
3 226 The mechanical efficiency of biting (the ratio of predicted bite force to input muscle force) at
4
5 227 each gape in the two species is given in Table 2. *Fukomys* is more efficient than *Bathyergus*
6
7 228 at converting input forces to output forces at all gape angles. As gape increases, mechanical
8
9 229 efficiency decreases in both specimens, but at different rates. Specifically, *Fukomys* is half as
10
11 230 efficient at 60° as at 0° whereas the mechanical efficiency of *Bathyergus* at 60° is only a
12
13 231 quarter of its efficiency at occlusion. It should be noted that the mechanical efficiency (and
14
15 232 thus bite force) of *Bathyergus* at 90° gape is negative. This is a result of many of the muscle
16
17 233 vectors rotating so far around that they now exert an upward rather than downward force on
18
19 234 the skull model, and is clearly a biologically unrealistic situation.
20
21
22 235
23
24
25 236 Figure 4 shows the size and shape deformations between the two model types at varying
26
27 237 degrees of gape. PC1 represents 76.27% variance and PC2 13.33%. PC1 is dominated by the
28
29 238 differences between the loaded models at differing angles of gape whilst PC2 shows the
30
31 239 difference between the unloaded mean and the loaded models. *Bathyergus* in occlusion and
32
33 240 *Fukomys* at 90° gape are the least deformed from the mean unloaded model; whereas
34
35 241 *Bathyergus* at 90° gape and *Fukomys* in occlusion are the most deformed from the mean
36
37 242 unloaded model. Figures 5A-C show the deformation between the mean unloaded model and
38
39 243 the two models at occlusion using thin plate splines. The main difference between the mean
40
41 244 unloaded model and the loaded models at occlusion is the ventral deflection of the zygomatic
42
43 245 arch. Figures 5D and E show cranial deformations from unloaded mean to 90° gape in both
44
45 246 models. The deformations between the two models are shown to be rather similar, with
46
47 247 increasing gapes being associated with dorsoventral bending.
48
49 248
50
51
52 249 **DISCUSSION**
53
54
55 250 *Von Mises stress*
56
57
58
59
60

251 The results of the FEA allow us to compare the biomechanical performance of the skull
252 between gapes within each model. Three performance metrics were studied: median VM
253 stress across the model; the ratio of predicted bite force to total input adductor muscle force;
254 and overall deformation of the model (following [20]). In both models, average VM stress
255 decreases as gape increases (Table 2). In particular, VM stress is reduced in the anterior part
256 of the skull (Figure 3), likely as a result of the muscle vectors being oriented in a more
257 posterior, rather than ventral, direction. At each gape, the *Bathyergerus* model experiences a
258 lower median stress than the *Fukomys* model, suggesting that the morphology of the
259 *Bathyergerus* cranium is better able to resist the forces applied to it in this analysis. This is
260 counter to the first hypothesis that suggested the chisel-tooth digging species would exhibit
261 lower stresses at wider gapes. However, we urge caution in interpreting this result as,
262 although the muscle forces were scaled to surface area to enable direct comparisons of stress
263 values [43], it only indicates how the cranial morphology responds to forces. In reality, there
264 are likely to be large differences in the muscle force to surface area ratio, as well as potential
265 differences in the relative proportions of the muscles and the bone material properties
266 between the two taxa.

267

268 It is unclear whether VM stress values really matter in an evolutionary context, as long as
269 they are below the yield strength of bone, and there is little evidence of cranial bone naturally
270 loading to failure [20]. Thus, assuming cranial stress is within a suitable safety factor, its
271 precise value may not be important. Previous work has suggested that bats adapt their crania
272 in favour of mechanical efficiency of biting, whereas adaptation to cranial strength (i.e. low
273 VM stress) is not as strongly selected for [45].

274

275 *Mechanical efficiency of biting*

1
2
3
4
5
6
7
8
9
10
11
12
13
14
15
16
17
18
19
20
21
22
23
24
25
26
27
28
29
30
31
32
33
34
35
36
37
38
39
40
41
42
43
44
45
46
47
48
49
50
51
52
53
54
55
56
57
58
59
60

276 From Table 2, it can be seen that the *Fukomys* model has a greater mechanical efficiency of
277 biting than the *Bathyergus* model at all simulated gapes, not just at wider gapes as predicted
278 in our second hypothesis. As would be expected from simple mechanics, bite force (and thus
279 mechanical efficiency) decreased with increasing gape in both models [46-49]. However, the
280 relative decrease with increasing gape was much greater in the *Bathyergus* model. That is, the
281 cranial morphology of *Fukomys* is better able to maintain mechanical efficiency as the
282 muscle forces rotate posteriorly. A higher mechanical efficiency can be partly achieved by
283 having masticatory muscles that have increased moment arms around the TMJ. Previous
284 work has indicated that the temporalis muscles of chisel-tooth digging bathyergids have
285 increased moment arms compared to *Bathyergus* [6] and therefore this could be the muscle
286 driving improved mechanical efficiency at increased gapes in the *Fukomys* model presented
287 here.

288
289 *Cranial deformation*

290 The GMM analysis shows that the relative deformation of the models at different gapes
291 follows an almost symmetrical pattern (Figure 4). The main difference between the two
292 models is that, as gape increases, the *Fukomys* model deforms less (plots closer to the
293 unloaded model) and the *Bathyergus* model deforms more (plots further from the unloaded
294 model). This result is as predicted by the third hypothesis and fits with the digging behaviour
295 of these two species. It appears that in *Fukomys* the morphology of the cranium leads to
296 reduced deformation at the wide gapes necessary for chisel-tooth digging [6,10]. *Bathyergus*,
297 as a scratch digger [2], does not employ such wide gapes as frequently, and thus its cranial
298 morphology deforms least at narrower gapes.

When comparing the two models at occlusion, it can be seen that the main difference in deformation occurs at the zygomatic arch, which is more ventrally deflected in *Fukomys* than *Bathyergus* (Figures 5B and C). As the models have been scaled to the same muscle force:surface area ratio, it is unlikely that the greater zygomatic deformation is a product of greater muscle force in *Fukomys*; rather, it is differences in the direction of muscle pull that appear to be leading to this result. It can be seen in Figure 1 that the deep masseter of *Bathyergus* has a greater posterior component to its line of action than does that of *Fukomys*. Thus the forces acting on the zygomatic arch of *Fukomys* are likely to produce a greater ventral deflection than is seen in *Bathyergus*.

Figures 5D and E represent how the models deform at large gape angles. Both models seem to experience dorsoventral bending of the cranium. As gape increases, the arrangement of the most dominant muscles (Figure 1), the temporalis (which attaches to the posterior area of the cranium) and masseters (which attach to the zygoma), will cause dorsoventral bending of the cranium around the TMJ constraints. Less bending will occur at the incisor as the muscle vectors rotate with the mandible as gape increases. This results in the muscle vectors directing more force towards the posterior part of the skull, and less force towards the anterior portion (this is also demonstrated by VM stress patterns in Figure 3 where cranial stress is concentrated at the posterior areas of the cranium as gape increases). Interestingly, the *Fukomys* model does not experience as much deformation or dorsoventral bending at 90° gape compared to *Bathyergus* (Figures 4 and 5D,E). This implies that the *Fukomys* cranium is stiffer than the *Bathyergus* cranium, which is to be expected from a cranium that has higher mechanical efficiency (Table 2). The stiffer the cranium is during mastication, the less energy it will waste in deforming, making it more efficient at converting muscle forces into bite forces.

1
2
3
4
5
6
7
8
9
10
11
12
13
14
15
16
17
18
19
20
21
22
23
24
25
26
27
28
29
30
31
32
33
34
35
36
37
38
39
40
41
42
43
44
45
46
47
48
49
50
51
52
53
54
55
56
57
58
59
60

325

326 *Conclusions*

327 The results here demonstrate that the cranial morphology of *Fukomys* performs better during
328 incisor biting at wide gapes than does *Bathyergus*. That is, the *Fukomys* model had a greater
329 mechanical efficiency of biting than *Bathyergus* and was able to maintain it to a greater
330 degree as gape increased. In addition, deformations of the *Fukomys* cranial model were
331 smaller at larger gapes, whereas in *Bathyergus* deformations were smaller at narrower gapes.
332 The relative performance of the models is congruent with the known digging behaviour of the
333 two species under study here i.e. chisel-tooth digging in *Fukomys* and scratch digging in
334 *Bathyergus* [2]. Previous studies of subterranean rodents have indicated that digging
335 behaviour has a major impact on cranial morphology [15,16] and that chisel-tooth digging
336 species have adaptations for high bite force and wide gape [6,10]. The cranial morphology of
337 the chisel-tooth digger in this analysis is clearly able to function well at wide gapes, and,
338 although absolute bite force cannot be predicted with any degree of confidence by our
339 unvalidated models, increasing the efficiency of the masticatory system would necessarily
340 increase bite force. It should be emphasised that the conclusions drawn here relate only to the
341 morphology of the cranium. To understand the biomechanics of digging more thoroughly
342 would require a much more complex model incorporating data on muscle physiology, bone
343 material properties, behaviour, and many other factors, which we feel would be a very fruitful
344 avenue of research.

345

346 **DATA ACCESSIBILITY.** Surface reconstructions, FE models and displacement files
347 available from https://figshare.com/articles/Mole_rat_FEA/3188830.

AUTHOR CONTRIBUTIONS. PGC conceived the study. AFM built and solved the models and analysed the data. Both authors interpreted the data. AFM drafted the manuscript. Both authors revised the manuscript and gave final approval for publication.

COMPETING INTERESTS. We have no competing interests.

FUNDING. AFM was funded by a University of Hull PhD studentship.

ACKNOWLEDGEMENTS. The authors would like to thank Professor Nigel Bennett (University of Pretoria) and Professor Christiane Denys and Dr Violaine Nicolas (Museum National d'Histoire Naturelle, Paris) for providing the specimens used in this study. We are grateful to Professor Michael Fagan and Mrs Sue Taft (University of Hull) for microCT scanning specimens. We thank Professor Nick Milne (University of Western Australia), and Professor Paul O'Higgins, Dr Sam Cobb, Dr Laura Fitton and Professor John Currey (University of York) for many stimulating and helpful conversations about this research.

REFERENCES

1. Faulkes CG, Bennett NC. 2013 Plasticity and constraints on social evolution in African mole-rats: ultimate and proximate factors. *Phil. Trans. R. Soc. B* **368**, 20120347.
2. Jarvis JUM, Bennett NC. 1991 Ecology and behaviour of the family Bathyergidae. In *The biology of the naked mole-rat* (eds PW Sherman, JUM Jarvis, RD Alexander), pp. 66-96. Princeton, NJ: Princeton University Press.
3. Stein BR. 2000 Morphology of subterranean rodents. In *Life underground: the biology of subterranean rodents* (eds EA Lacey, JL Patton, GN Cameron), pp. 19-61. Chicago: University of Chicago Press.
4. Lessa EP, Thaler CS. 1989 A reassessment of morphological specializations for digging in pocket gophers. *J. Mammal.* **70**, 689-700.

1
2
3
4
5
6
7
8
9
10
11
12
13
14
15
16
17
18
19
20
21
22
23
24
25
26
27
28
29
30
31
32
33
34
35
36
37
38
39
40
41
42
43
44
45
46
47
48
49
50
51
52
53
54
55
56
57
58
59
60

373 5. Samuels JX, Van Valkenburgh B. 2009 Craniodental adaptations for digging in
374 extinct burrowing beavers. *J. Vert. Paleo.* **29**, 254-268.

375 6. McIntosh AF, Cox PG. 2016 Functional implications of craniomandibular
376 morphology in African mole-rats (Rodentia: Bathyergidae). *Biol. J. Linn. Soc.* **117**,
377 447-462.

378 7. Landry SO. 1957 Factors affecting the procumbency of rodent upper incisors. *J.*
379 *Mammal.* **38**, 223-234.

380 8. Agrawal V. 1967 Skull adaptations in fossorial rodents. *Mammalia* **31**, 300-312.

381 9. Lessa EP, Stein BR. 1992 Morphological constraints in the digging apparatus of
382 pocket gophers (Mammalia: Geomyidae). *Biol. J. Linn. Soc.* **47**, 439-453.

383 10. Gomes Rodrigues H, Šumbera R, Hautier L. 2016 Life in burrows channelled the
384 morphological evolution of the skull in rodents: the case of African mole-rats
385 (Bathyergidae, Rodentia). *J. Mamm. Evol.* **23**, 175-189.

386 11. Verzi DH, Olivares AI. 2006 Craniomandibular joint in South American burrowing
387 rodents (Ctenomyidae): adaptations and constraints related to a specialized
388 mandibular position in digging. *J. Zool.* **270**, 488-501.

389 12. Wroe S, McHenry C, Thomason J. 2005 Bite club: comparative bite force in big
390 biting mammals and the prediction of predatory behaviour in fossil taxa. *Proc. R. Soc.*
391 *B* **272**, 619-625.

392 13. Wroe S, Milne N. 2007 Convergence and remarkably consistent constraint in the
393 evolution of carnivore skull shape. *Evolution* **61**, 1251-1260.

394 14. Figueirido B, Tseng ZJ, Martín-Serra A. 2013 Skull shape evolution in durophagous
395 carnivorans. *Evolution* **67**, 1975-1993.

- 396 15. Barčiová L, Šumbera R, Burda H. 2009 Variation in the digging apparatus of the
397 subterranean silvery mole-rat *Heliophobius argenteocinereus* (Rodentia,
398 Bathyergidae): the role of ecology and geography. *Biol. J. Linn. Soc.* **97**, 822-831.
- 399 16. Beolchini F, Corti M. 2004 The taxonomy of the genus *Tachyoryctes*: a geometric
400 morphometric approach. *It. J. Zool.* **71**, 35-43.
- 401 17. Rayfield EJ. 2004 Cranial mechanics and feeding in *Tyrannosaurus rex*. *Proc. R. Soc.*
402 *B* **271**, 1451-59.
- 403 18. Strait DS, Wang Q, Dechow PC, Ross CF, Richmond BG, Spencer MA, Patel BA.
404 2005 Modeling elastic properties in finite-element analysis: how much precision is
405 needed to produce an accurate model? *Anat. Rec.* **283A**, 275-287.
- 406 19. Kupczik K, Dobson CA, Fagan MJ, Crompton RH, Oxnard CE, O'Higgins P. 2007
407 Assessing mechanical function of the zygomatic region in macaques: validation and
408 sensitivity testing of finite element models. *J. Anat.* **210**, 41-53.
- 409 20. Dumont ER, Davis JL, Grosse IR, Burrows AM. 2011 Finite element analysis of
410 performance in the skulls of marmosets and tamarins. *J. Anat.* **218**, 151-162.
- 411 21. Cox PG, Rayfield EJ, Fagan MJ, Herrel A, Pataky TC, Jeffery N. 2012 Functional
412 evolution of the feeding system in rodents. *PLoS ONE*, **7**, e36299.
- 413 22. O'Higgins P, Fitton L, Phillips R, Shi J, Liu J, Gröning F, Cobb S, Fagan MJ. 2012
414 Virtual functional morphology: novel approaches to the study of craniofacial form
415 and function. *Evol. Biol.* **39**, 521-535.
- 416 23. Cox PG, Kirkham J, Herrel A. 2013 Masticatory biomechanics of the Laotian rock
417 rat, *Laonastes aenigmamus*, and the function of the zygomaticomandibularis muscle.
418 *PeerJ* **1**, e160.
- 419 24. O'Hare LMS, Cox PG, Jeffery N, Singer ER. 2013 Finite element analysis of stress in
420 the equine proximal phalanx. *Equine Vet. J.* **45**, 273-277.

1
2
3
4
5
6
7
8
9
10
11
12
13
14
15
16
17
18
19
20
21
22
23
24
25
26
27
28
29
30
31
32
33
34
35
36
37
38
39
40
41
42
43
44
45
46
47
48
49
50
51
52
53
54
55
56
57
58
59
60

25. Cox PG, Rinderknecht A, Blanco RE. 2015 Predicting bite force and cranial biomechanics in the largest fossil rodent using finite element analysis. *J. Anat.* **226**, 215-223.

26. Fitton LC, Prôa M, Rowland C, Toro-Ibacache V, O'Higgins P. 2015 The impact of simplifications on the performance of a finite element model of a *Macaca fascicularis* cranium. *Anat. Rec.* **298**, 107-121.

27. Rayfield EJ. 2007 Finite element analysis and understanding the biomechanics and evolution of living and fossil organisms. *Ann. Rev. Earth Planet. Sci.* **35**, 541-576.

28. Bright JA, Rayfield EJ. 2011 Sensitivity and *ex vivo* validation of finite element models of the domestic pig cranium. *J. Anat.* **219**, 456-471.

29. Porro LB, Metzger KA, Iriarte-Diaz J, Ross CF. 2013 *In vivo* bone strain and finite element modelling of the mandible of *Alligator mississippiensis*. *J. Anat.* **223**, 195-227.

30. O'Higgins P, Cobb SN, Fitton LC, Gröning F, Phillips R, Liu J, Fagan MJ. 2011 Combining geometric morphometrics and functional simulation: an emerging toolkit for virtual functional analyses. *J. Anat.* **218**, 3-15.

31. Liu J, Shi J, Fitton L, Phillips R, O'Higgins P, Fagan MJ. 2012 The application of muscle wrapping to voxel-based finite element models of skeletal structures. *Biomech. Model. Mechanobiol.* **11**, 35-47.

32. Cox PG, Fagan MJ, Rayfield EJ, Jeffery N. 2011 Finite element modelling of squirrel, guinea pig and rat skulls: using geometric morphometrics to assess sensitivity. *J. Anat.* **219**, 696-709.

33. Williams KR, Edmundson JT. 1984 Orthodontic tooth movement analysed by the finite element method. *Biomaterials* **5**, 347-351.

- 1
2
3 445 34. Turnbull WD. 1970 Mammalian masticatory apparatus. *Fieldiana (Geol.)* **18**, 147-
4
5 446 356.
6
7 447 35. Cox PG, Jeffery N. 2011 Reviewing the morphology of the jaw-closing musculature
8
9 448 in squirrels, rats, and guinea pigs with contrast-enhanced microCT. *Anat. Rec.* **294**,
10 449 915-928.
11
12 450 36. Boller N. 1970 Untersuchungen an Schädel, Kaumuskulatur und äußerer Hirnform
13
14 451 von *Cryptomys hottentotus* (Rodentia, Bathyergidae). *Z. wiss. Zool.* **181**, 7-65.
15
16 452 37. Morlok WF. 1983 Vergleichend- und funktionell-anatomische Untersuchungen an
17
18 453 Kopf, Hals und Vorderextremität subterranean Nagetiere (Mammalia, Rodentia). *Cour.*
19 454 *Forsch. Inst. Senck.* **64**, 1-237.
20
21 455 38. Van Daele P, Herrel A, Adriaens D. 2009 Biting performance in teeth-digging
22 456 African mole-rats (*Fukomys*, Bathyergidae, Rodentia). *Physiol. Biochem. Zool.* **82**,
23 457 40-50.
24
25 458 39. Cox PG, Faulkes CG. 2014 Digital dissection of the masticatory muscles of the naked
26 459 mole-rat, *Heterocephalus glaber* (Mammalia, Rodentia). *PeerJ* **2**, e448.
27
28 460 40. Offermans M, de Vree F. 1990 Mastication in springhares, *Pedetes capensis*: a
29 461 cineradiographic study. *J. Morphol.* **205**, 353-367.
30
31 462 41. Satoh K. 1998 Balancing function of the masticatory muscles during incisal biting in
32 463 two murid rodents, *Apodemus speciosus* and *Clethrionomys rufocanus*. *J. Morphol.*
33 464 **236**, 49-56.
34
35 465 42. Weijs W, Hillen B. 1985 Cross-sectional areas and estimated intrinsic strength of the
36 466 human jaw muscles. *Acta Morphol. Neerl. Scand.* **23**, 267-274.
37
38 467 43. Dumont ER, Grosse IR, Slater GJ. 2009 Requirements for comparing the performance
39 468 of finite element models of biological structures. *J. Theor. Biol.* **256**, 96-103.
40
41
42
43
44
45
46
47
48
49
50
51
52
53
54
55
56
57
58
59
60

1
2
3 469 44. O'Higgins P, Milne N. 2013 Applying geometric morphometrics to compare changes
4
5 470 in size and shape arising from finite elements analyses. *Hystrix* **24**, 126-132.
6
7 471 45. Dumont ER, Samadevam K, Grosse I, Warsi OM, Baird B, Davalos LM. 2014
8
9 472 Selection for mechanical advantage underlies multiple cranial optima in new world
10
11 473 leaf-nosed bats. *Evolution* **68**, 1436-1449.
12
13 474 46. Herring SW, Herring SE. 1974 The superficial masseter and gape in mammals. *Am.*
14
15 475 *Nat.* **108**, 561-576.
16
17 476 47. Dumont ER, Herrel A. 2003 The effects of gape angle and bite point on bite force in
18
19 477 bats. *J. Exp. Biol.* **206**, 2117-2123.
20
21 478 48. Bourke J, Wroe S, Moreno K, McHenry C, Clausen P. 2008 Effects of gape and tooth
22
23 479 position on bite force and skull stress in the dingo (*Canis lupus dingo*) using a 3-
24
25 480 dimensional finite element approach. *PLoS ONE*, **3**, e2200.
26
27 481 49. Williams SH, Peiffer E, Ford S. 2009 Gape and bite force in the rodents *Onychomys*
28
29 482 *leucogaster* and *Peromyscus maniculatus*: does jaw-muscle anatomy predict
30
31 483 performance? *J. Morphol.* **270**, 1338-1347.
32
33
34
35
36
37
38

39 **FIGURE LEGENDS**
40
41 **Figure 1.** Attachment sites and vectors of pull of the masticatory muscles in models of
42
43 *Bathyergus suillus*, in (A) right lateral and (B) ventral view, and *Fukomys mechowii*, in (C)
44
45 right lateral and (D) ventral view. Colours of muscle origins and vectors: temporalis, red;
46
47 superficial masseter, cyan; deep masseter, royal blue; IOZM, green; anterior ZM, purple;
48
49 posterior ZM, yellow; lateral pterygoid, brown; medial pterygoid, orange.
50
51
52
53
54 **Figure 2.** Landmark configuration represented on *Fukomys mechowii* in (A) dorsal, (B)
55
56 ventral, and (C) left lateral view. Text definitions of landmarks given in Table S1.
57
58
59
60

494

495 **Figure 3.** Predicted von Mises stress distributions across the skulls of *Fukomys* (left column)
496 and *Bathyergus* (right column) during incisor biting at four different gape angles.

497

498 **Figure 4.** PCA plot representing the differences of deformations between the two models
499 scaled to force:area ratio. Key: cross, mean unloaded model; blue shapes, *Fukomys* models;
500 red shapes, *Bathyergus* models; circles, occlusion; triangles, 30° gape; squares, 60° gape;
501 diamonds, 90° gape.

502

503 **Figure 5.** Transformation grids and surface warps associated with PCA plot (Figure 4)
504 representing the differences of deformation between the two models scaled to force:area
505 ratio. Arrows represent the change in size and shape between unloaded mean model and
506 target. A, unloaded mean model; B, size and shape change from unloaded model to *Fukomys*
507 model in occlusion; C, size and shape change from unloaded model to *Bathyergus* model in
508 occlusion; D, size and shape change from unloaded model to *Fukomys* model at 90° gape; E,
509 size and shape change from unloaded model to *Bathyergus* model at 90° gape.

510

511

512 TABLE CAPTIONS

513 **Table 1.** Muscle loads applied to each side of the finite element models of *Fukomys*
514 *mechowii* and *Bathyergus suillis*.

515

516 **Table 2.** Median von Mises stress and mechanical efficiency of biting in *Fukomys mechowii*
517 and *Bathyergus suillis* at increasing gape.

Table 1. Muscle loads applied to each side of the finite element models of *Fukomys mehowi* and *Bathyergus suillis*.

Muscle	Force (N)	
	<i>Fukomys</i>	<i>Bathyergus</i>
Temporalis	20.7	24.1
Superficial masseter	6.3	7.3
Deep masseter	11.7	13.6
Anterior ZM	1.5	1.7
Posterior ZM	1.5	1.7
Infraorbital ZM	3.0	3.5
Medial pterygoid	5.1	6.0
Lateral pterygoid	3.3	3.8

Table 2. Median von Mises stress and mechanical efficiency of biting in *Fukomys mehowi* and *Bathyergus suillis* at increasing gape.

Gape angle (°)	Median VM (MPa)		Mechanical efficiency	
	<i>Fukomys</i>	<i>Bathyergus</i>	<i>Fukomys</i>	<i>Bathyergus</i>
0	1.06	0.88	0.18	0.13
30	1.04	0.76	0.15	0.08
60	0.85	0.52	0.09	0.03
90	0.63	0.59	0.02	-0.03

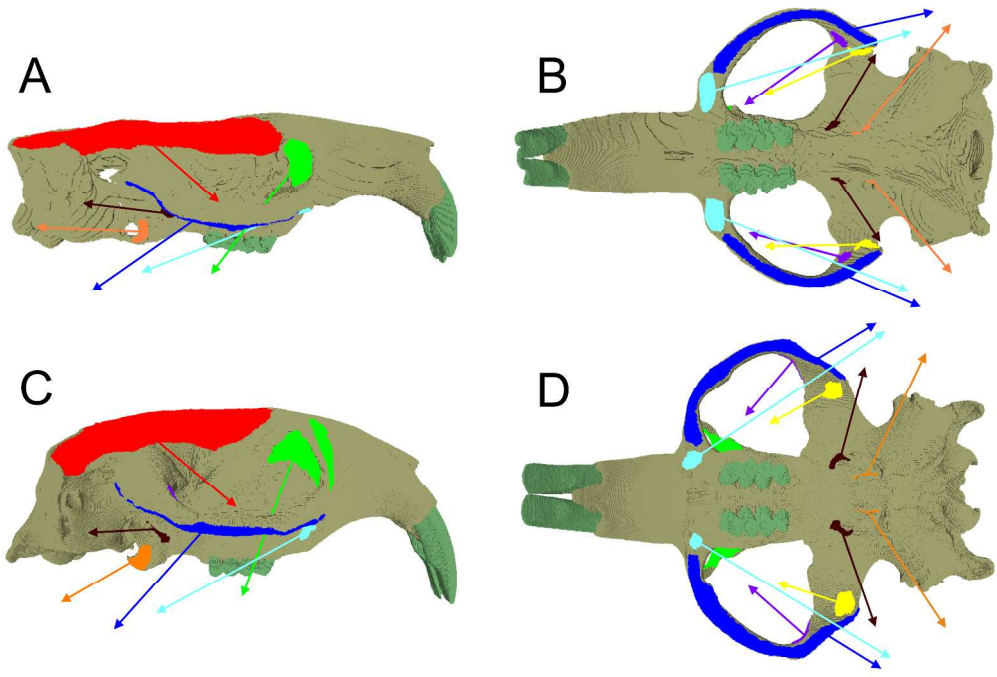


Figure 1. Attachment sites and vectors of pull of the masticatory muscles in models of *Bathyergus suillus*, in (A) right lateral and (B) ventral view, and *Fukomys mechowii*, in (C) right lateral and (D) ventral view. Colours of muscle origins and vectors: temporalis, red; superficial masseter, cyan; deep masseter, royal blue; IOZM, green; anterior ZM, purple; posterior ZM, yellow; lateral pterygoid, brown; medial pterygoid, orange.

170x116mm (600 x 600 DPI)

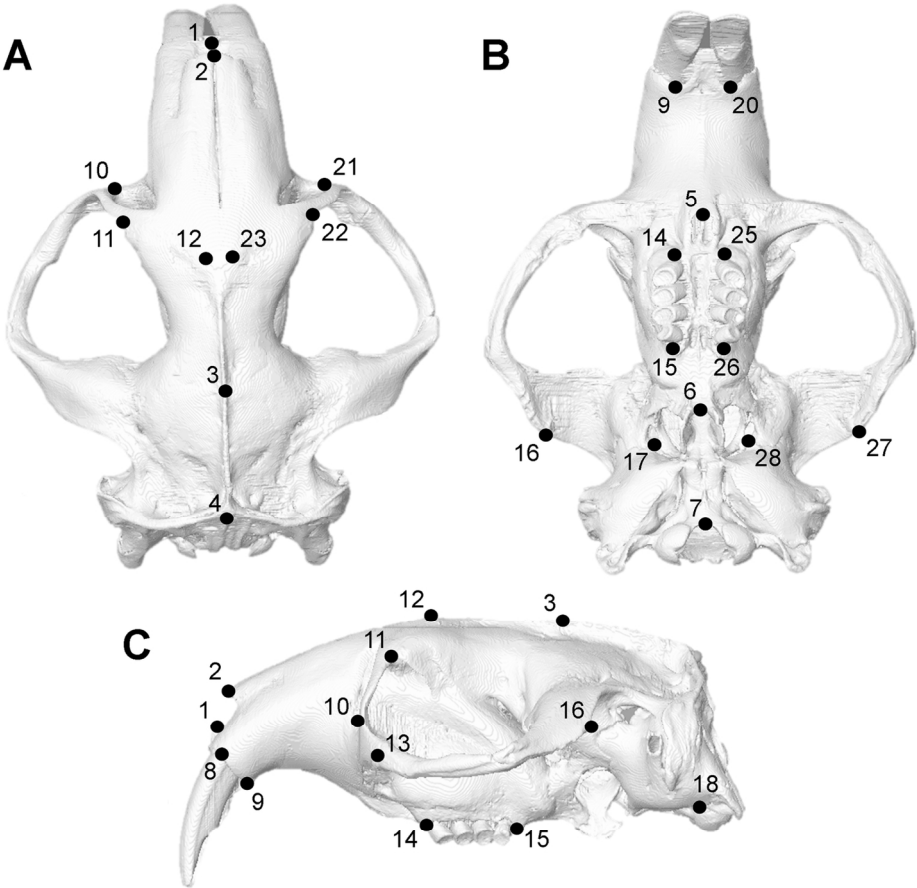


Figure 2. Landmark configuration represented on *Fukomys mechowii* in (A) dorsal, (B) ventral, and (C) left lateral view. Text definitions of landmarks given in Table S1.

140x131mm (300 x 300 DPI)

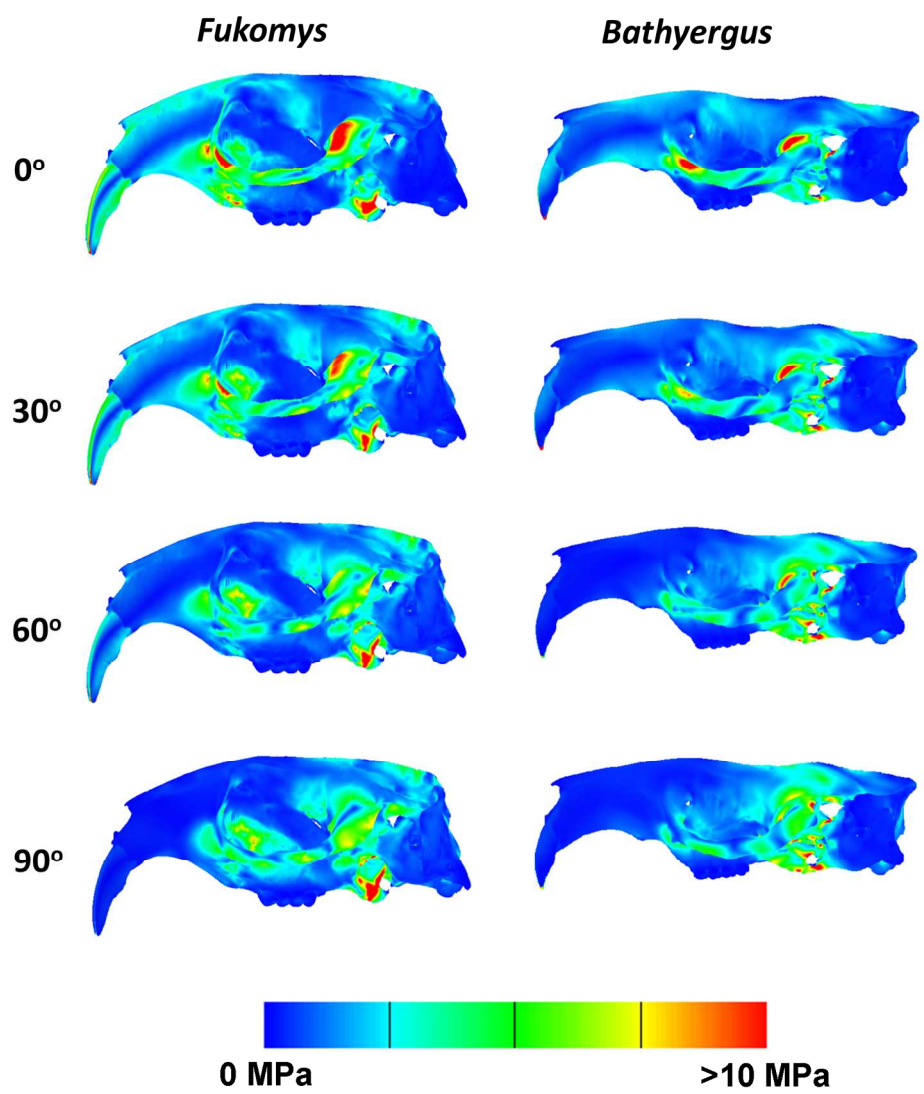


Figure 3. Predicted von Mises stress distributions across the skulls of *Fukomys* (left column) and *Bathyergus* (right column) during incisor biting at four different gape angles.

174x207mm (283 x 283 DPI)

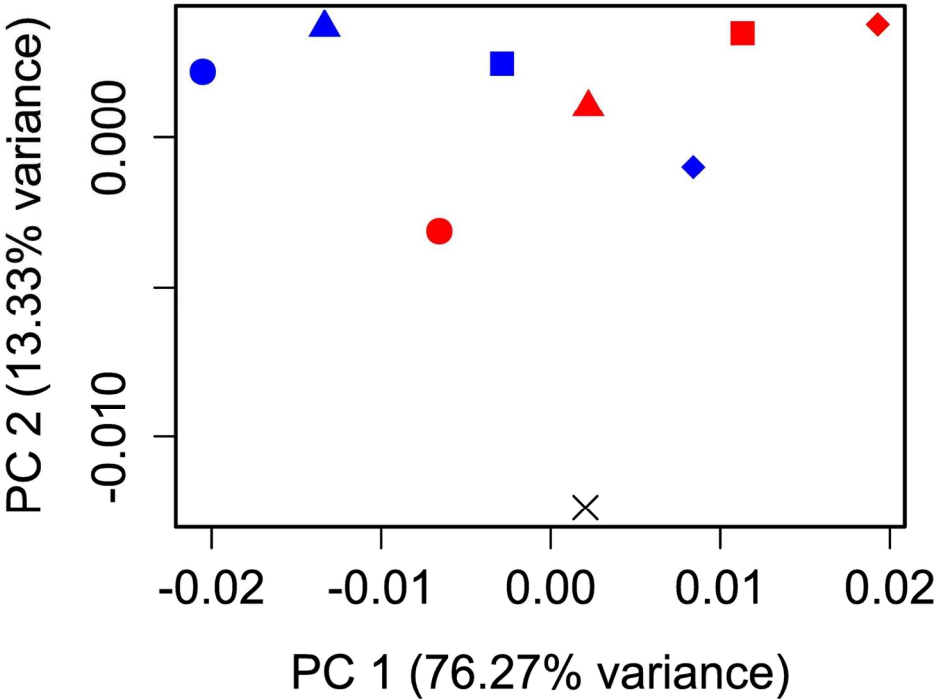


Figure 4. PCA plot representing the differences of deformations between the two models scaled to force:area ratio. Key: cross, mean unloaded model; blue shapes, *Fukomys* models; red shapes, *Bathyergus* models; circles, occlusion; triangles, 30° gape; squares, 60° gape; diamonds, 90° gape.

143x114mm (300 x 300 DPI)

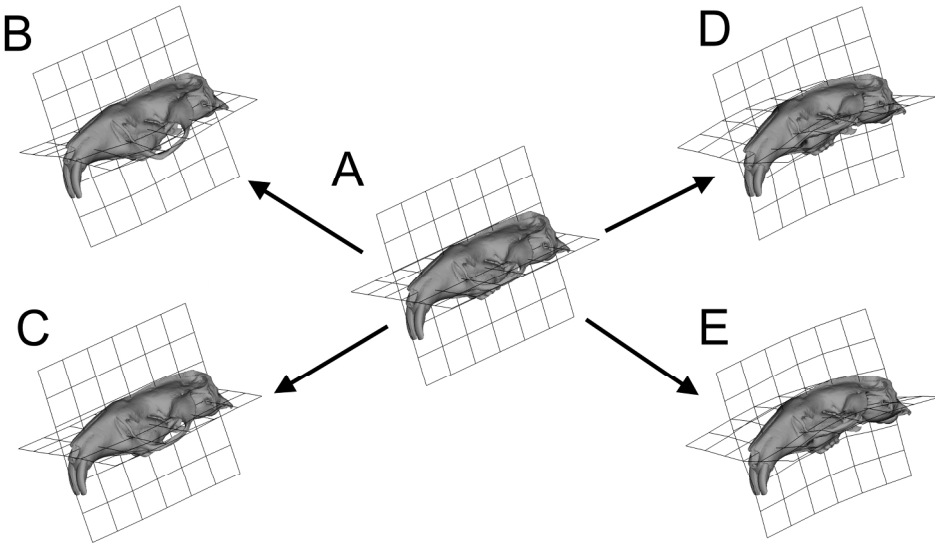


Figure 5. Transformation grids and surface warps associated with PCA plot (Figure 4) representing the differences of deformation between the two models scaled to force:area ratio. Arrows represent the change in size and shape between unloaded mean model and target. A, unloaded mean model; B, size and shape change from unloaded model to *Fukomys* model in occlusion; C, size and shape change from unloaded model to *Bathyergus* model in occlusion; D, size and shape change from unloaded model to *Fukomys* model at 90° gape; E, size and shape change from unloaded model to *Bathyergus* model at 90° gape.